Bulk and single-particle properties of hyperonic matter at finite temperature

A. Rios,[1] A. Polls,[1] A. Ramos,[1] and I. Vidaña[2]
[1]*Departament d'Estructura i Constituents de la Matèria, Universitat de Barcelona, Avda. Diagonal 647, E-08028 Barcelona, Spain*
[2]*Gesellschaft für Schwerionenforschung (GSI), Planckstrasse 1, D-64291 Darmstadt, Germany*
(Received 29 March 2005; published 25 August 2005)

Bulk and single-particle properties of hot hyperonic matter are studied within the Brueckner-Hartree-Fock approximation extended to finite temperature. The bare interaction in the nucleon sector is the Argonne V18 potential supplemented with an effective three-body force to reproduce the saturating properties of nuclear matter. The modern Nijmegen NSC97e potential is employed for the hyperon-nucleon and hyperon-hyperon interactions. The effect of temperature on the in-medium effective interaction is found to be, in general, very small and the single-particle potentials differ by at most 25% for temperatures in the range from 0 to 60 MeV. The bulk properties of infinite matter of baryons, either nuclear isospin symmetric or a β-stable composition that includes a nonzero fraction of hyperons, are obtained. It is found that the presence of hyperons can modify the thermodynamical properties of the system in a non-negligible way.

DOI: 10.1103/PhysRevC.72.024316 PACS number(s): 26.60.+c, 21.65.+f, 13.75.Ev, 21.30.−x

I. INTRODUCTION

The equation of state (EoS) is the essential ingredient for understanding the behavior of nuclear matter under extreme conditions of density and temperature. Recently it has received renewed interest because of the possibility of attaining such conditions in relativistic heavy-ion collisions at GSI, CERN, and Brookhaven [1–3]. In these conditions, matter is expected to be at high densities and very high temperatures. The EoS for larger densities and lower temperatures is also important for the study of hot dense matter in astrophysical conditions [4]. Supernova models involve the gravitational collapse of the inner core of a massive star followed by the explosive ejection of the overlying material and the later formation of a proto-neutron star. During the collapse, matter reaches densities beyond nuclear matter saturation density ($\sim$0.17 fm^{-3}) and temperatures of several tens of MeV. Therefore, the description of matter in such conditions of density and temperature demands the introduction of new degrees of freedom other than those of nucleons. In the case of cold neutron stars (i.e., once neutrinos have been emitted and the temperature has dropped to negligible values), very different models have been used to describe their dense interior, ranging from quark matter to pion or kaon condensates. Special attention has been focused on the presence of hyperons (Λ and Σ^-) in such media and several calculations have been performed at $T = 0$, and at finite temperatures as well, within different phenomenological approaches [5,6] and relativistic mean-field models [7–10]. Microscopic calculations have also been widely applied to the study of cold neutron stars [11–16]. However, only a few microscopic calculations of the EoS at finite temperature are available [17–22] and, to the best of our knowledge, the present work is the first microscopic calculation of the EoS at finite temperatures that includes baryonic degrees of freedom other than nucleons.

The microscopic approach employed in this work is based on the Brueckner-Bethe-Goldstone (BBG) many-body theory. The basic input of our calculations is the baryon-baryon interaction for the complete baryon octet. For the nucleon-nucleon (NN) sector (i.e, for neutrons n and protons p) we use the realistic Argonne V18 (Av18) potential [23]. Nevertheless, since it is well known that a Brueckner-Hartree-Fock (BHF) approach with any realistic two-body interaction does not yield satisfactory saturation properties, we follow Refs. [17,18] and supplement it with a three-body force (TBF), which, after a suitable integration on the third particle, can be reduced to an effective two-body NN interaction. The nucleonic bulk properties are then very well described. However, for the hyperon-nucleon (YN) and hyperon-hyperon (YY) sectors, we use the Nijmegen NSC97e potential developed by Stoks and Rijken [24]. In our microscopic treatment, temperature effects are taken into account by modifying the momentum distributions and Pauli blocking factors appropriately and solving the problem self-consistently for a given density and temperature. In this way, the effective in-medium interaction, the single-particle properties, and the bulk observables are modified by temperature. This corresponds to the "naive" finite-temperature BBG (NTBBG) expansion referred to in Ref. [18], where it was found to be good enough for the low temperatures (up to $\sim$30 MeV) explored in that work.

The paper is organized in the following way. A brief review of the BHF approximation of the BBG many-body theory at zero temperature extended to the hyperonic sector is given in Sec. II A. The extension to the finite-temperature case is presented in Sec. II B. Section III is devoted to the presentation and discussion of the results. In Sec. III A we discuss the results related to the single-particle properties, whereas Sec. III B is devoted to the bulk properties of the system. Finally, a short summary and the main conclusions of this work are presented in Sec. IV.

II. FORMALISM

A. Zero-temperature BHF approximation

Our many-body scheme is based on the BHF approximation of the BBG theory extended to the hyperonic sector [11–13]. It starts with the construction of all the baryon-baryon

(i.e., NN, YN, and YY) G matrices, which describe in an effective way the interactions between baryons in the presence of a surrounding baryonic medium. They are formally obtained by solving the well-known Bethe-Goldstone equation, written schematically as

$$G(\omega)_{B_1B_2,B_3B_4} = V_{B_1B_2,B_3B_4} + \sum_{B_5B_6} V_{B_1B_2,B_5B_6} \times \frac{Q_{B_5B_6}}{\omega - E_{B_5} - E_{B_6} + i\eta} G(\omega)_{B_5B_6,B_3B_4}. \quad (1)$$

In this expression the first (last) two subindices indicate the initial (final) two-baryon states compatible with a given value S of the strangeness, namely, NN for $S = 0$, YN for $S = -1, -2$, and YY for $S = -2, -3, -4$; V is the bare baryon-baryon interaction (Av18 + TBF for NN; NSC97e for YN and YY); $Q_{B_5B_6}$ is the Pauli operator, which prevents the intermediate baryons B_5 and B_6 from being scattered to states below their respective Fermi momenta; and the starting energy ω corresponds to the sum of nonrelativistic single-particle energies of the interacting baryons (see Ref. [13] for computational details).

The single-particle energy of a baryon B_i is given by (in units in which $\hbar = 1$ and $c = 1$)

$$E_{B_i} = M_{B_i} + \frac{k^2}{2M_{B_i}} + \mathrm{Re}\left[U_{B_i}(k)\right], \quad (2)$$

where M_{B_i} denotes the rest mass of the baryon and the real part of the single-particle potential $U_{B_i}(k)$ represents the averaged field "felt" by the baryon owing to its interaction with the other baryons of the medium. In the BHF approximation, $U_{B_i}(k)$ is given by

$$U_{B_i}(k) = \sum_{B_j} \sum_{k'} n_{B_j}(k') \times \langle \vec{k}\vec{k}' | G_{B_iB_j,B_iB_j}\left(\omega = E_{B_i} + E_{B_j}\right) | \vec{k}\vec{k}' \rangle, \quad (3)$$

where

$$n_{B_j}(k) = \begin{cases} 1, & \text{if } k \leqslant k_{F_{B_j}} \\ 0, & \text{otherwise} \end{cases} \quad (4)$$

is the corresponding occupation number of the species B_j, a sum over all the different baryon species is performed, and the matrix elements are properly antisymmetrized when baryons B_i and B_j belong to the same isomultiplet. We note here that the so-called continuous prescription has been adopted for the single-particle potentials when solving the Bethe-Goldstone-equation at $T = 0$. As shown by the authors of Refs. [25, 26], the contribution to the energy per particle from three-body clusters is diminished in this prescription with respect to the one calculated with the gap choice for the single-particle potential. We note also that the present calculations have been carried out using the Av18 potential supplemented with a TBF in the NN sector and including the most recent parametrization of the bare baryon-baryon potential for the YN and YY sectors, as defined by Stoks and Rijken in Ref. [24]. This potential model, which aims at describing all interaction channels with strangeness from $S = 0$ to $S = 4$, is based on SU(3) extensions of the Nijmegen NN and YN potentials [27].

The calculations of all the other bulk properties of the cold system can then be obtained from the total energy per particle, E/A, which in the BHF approximation to the BBG expansion is given by

$$\frac{E}{A} = \frac{1}{A} \sum_{B_i} \sum_{k} n_{B_i}(k) \left\{ \frac{k^2}{2M_{B_i}} + \frac{1}{2} \sum_{B_j} \sum_{k'} n_{B_j}(k') \times \mathrm{Re}\left[\langle \vec{k}\vec{k}' | G_{B_iB_j,B_iB_j}\left(\omega = E_{B_i} + E_{B_j}\right) | \vec{k}\vec{k}' \rangle \right] \right\}, \quad (5)$$

once a self-consistent solution of Eqs. (1)–(3) is achieved.

B. Finite-temperature effects

The many-body problem at finite temperature has been considered by several authors within different approaches, such as the finite-temperature Green's function method [28], thermo-field dynamics [29], or the Bloch–De Dominicis (BD) diagrammatic expansion [30]. The latter, developed soon after the Brueckner theory, represents the "natural" extension to finite temperature of the BBG expansion, to which it leads in the zero-temperature limit. Baldo and Ferreira [18] showed that the dominant terms in the BD expansion were those that correspond to the zero-temperature BBG diagrams but introducing the temperature in the Fermi-Dirac distributions, which now read

$$f_{B_i}(k, T) = \frac{1}{1 + \exp\left(\left[E_{B_i}(k, T) - \widetilde{\mu}_{B_i}\right]/T\right)}, \quad (6)$$

where $\widetilde{\mu}_{B_i}$ is the chemical potential of the baryon species B_i.

Therefore, at the BHF level, finite-temperature effects can be introduced in a very good approximation just by changing in the Bethe-Goldstone equation (i) the zero-temperature Pauli operator $Q_{B_5B_6} = (1 - n_{B_5})(1 - n_{B_6})$ by the corresponding finite-temperature one $Q_{B_5B_6}(T) = (1 - f_{B_5})(1 - f_{B_6})$ and (ii) the single-particle energies E_{B_i} by the temperature-dependent ones $E_{B_i}(T)$ obtained from Eqs. (2) and (3) by replacing $n_{B_i}(k)$ by $f_{B_i}(k, T)$. These approximations, which we will presume to be valid in the range of densities and temperatures considered here, were referred to in [18] as the NTBBG expansion.

In this case, however, the self-consistent process implies that, together with the Bethe-Goldstone equation and the single-particle potentials, the chemical potential of each baryon species, $\widetilde{\mu}_{B_i}$, must be extracted at each step of the iterative process from the normalization condition

$$\rho_{B_i} = \sum_{k} f_{B_i}(k, T). \quad (7)$$

This is an implicit equation for each one of the chemical potentials, which can be solved numerically. Note that, now, also the Bethe-Goldstone equation and single-particle potentials depend implicitly on the chemical potentials.

Once a self-consistent solution is obtained, the total free energy per particle is determined by

$$\frac{F}{A} = \frac{E}{A} - T\frac{S}{A}, \quad (8)$$

where E/A is evaluated from Eq. (5) by replacing $n_{B_i}(k)$ by $f_{B_i}(k, T)$ and the total entropy per particle, S/A, is calculated

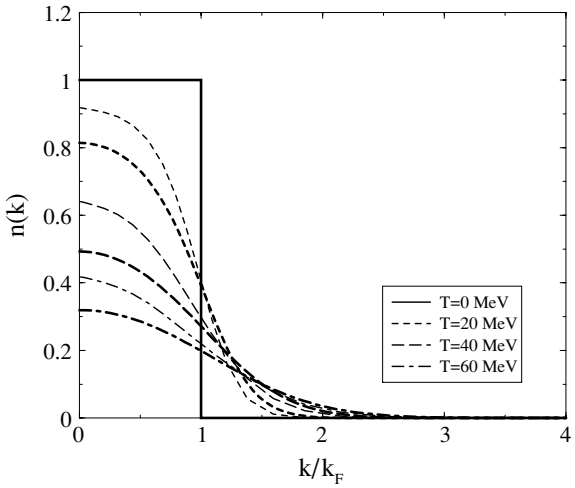

FIG. 1. Nucleon momentum distributions at ρ_0 for various temperatures: $T = 0, 20, 40$, and 60 MeV. The thick lines have been obtained with a purely kinetic energy spectrum; the thin lines contain the effect of a single-particle potential.

using the following mean-field expression:

$$\frac{S}{A} = -\frac{1}{A}\sum_{B_i}\sum_{k}\{f_{B_i}(k,T)\ln[f_{B_i}(k,T)] + [1-f_{B_i}(k,T)]\ln[1-f_{B_i}(k,T)]\}. \quad (9)$$

We note that in a thermodynamically consistent (conserving) approach, the value of the chemical potential $\widetilde{\mu}_{B_i}$ obtained from the normalization condition (6) should coincide with the thermodynamical definition

$$\mu_{B_i} = \frac{\partial F}{\partial N_{B_i}}. \quad (10)$$

This is not the case for the BHF approximation employed here, neither at zero nor at finite temperature, as is well known. Another manifestation of the nonconserving character of the BHF approach is the violation of the Hugenholtz-van Hove theorem. Further remarks on this problem and how the validity of the Hugenholtz-van Hove theorem can be restored will be given in the next section.

III. RESULTS

A. Single-particle properties

We start this section by discussing the behavior of the momentum distribution and the Pauli operator with temperature, since both are crucial ingredients in determining the dependence with temperature of all the other physical quantities. The momentum distribution in nuclear matter at experimental saturation density $\rho_0 = 0.17$ fm^{-3} is shown in Fig. 1 for various temperatures from $T = 0$ MeV to $T = 60$ MeV. The thick lines are momentum distributions obtained with a purely kinetic energy spectrum and will be denoted by $f_{\text{free}}(k,T)$ henceforth. The thin lines, which will be denoted as $f(k,T)$, contain the effect of a single-particle potential. It may appear surprising that the depletion of low-momentum states for a noninteracting system at finite temperature is larger than that for the interacting system at the same temperature [i.e., $f_{\text{free}}(0,T) < f(0,T)$]. This is a direct consequence of the momentum dependence of the spectrum and it is the behavior to be expected for nucleons in nuclear matter, which have a steeper spectrum than the purely kinetic energy one, hence making the single-particle excitations more costly than in the free system.

The corresponding angle-averaged Pauli blocking factor between two different baryons B_1 and B_2 reads

$$\bar{Q}_{B_1B_2}(k,K) = \frac{1}{2}\int_{-1}^{1} d(\cos\theta)\left[1-f_{B_1}(|\,\alpha\vec{K}+\vec{k}\,|,T)\right] \times\left[1-f_{B_2}(|\,\beta\vec{K}-\vec{k}\,|,T)\right], \quad (11)$$

where $\alpha = M_1/(M_1+M_2)$ and $\beta = M_2/(M_1+M_2)$. In Fig. 2, we show the nucleon-nucleon Pauli blocking factor as a function of relative momentum k and for two different total momenta, $K = 0$ (left panel) and $K = 3k_F$ (right panel), calculated at the previously stated density and temperatures. One can see that the sharp behaviors that characterized the Pauli blocking at zero temperature smear out considerably with

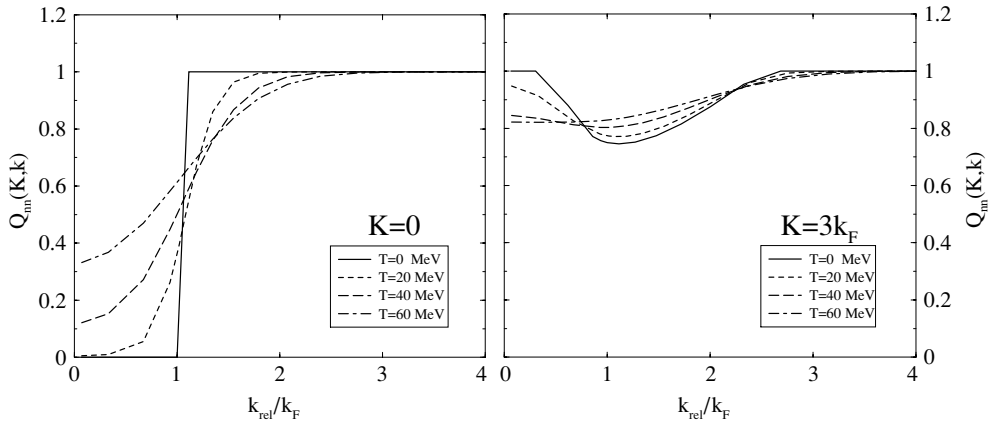

FIG. 2. Pauli blocking factor at ρ_0 for various temperatures: $T = 0, 20, 40$, and 60 MeV. The center-of-mass momenta are $K = 0$ fm^{-1} (left panel) and $K = 3k_F$ fm^{-1} (right panel).

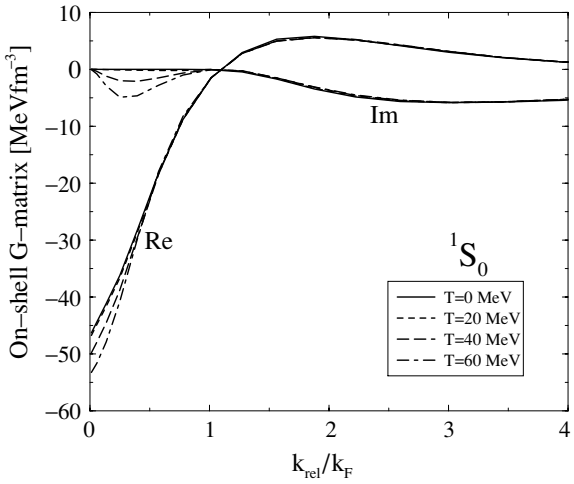

FIG. 3. $^1S_0$ on-shell G-matrix elements as a function of relative momentum at ρ_0 for various temperatures: $T = 0, 20, 40,$ and 60 MeV.

temperature. In addition, the figure also illustrates the loss of Pauli blocking effects as temperature increases. Because of this gain in phase space, medium effects weaken with increasing temperature.

We next discuss the behavior of the NN effective in-medium interaction with temperature. The $^1S_0$ G-matrix element is shown in Fig. 3 as a function of the on-shell relative momemtum for a total center-of-mass momentum $K = 0$. Whereas the real part shows little dependence with temperature, the imaginary part reflects in a more explicit way the behavior of the Pauli blocking factor. At finite temperature, a nonzero imaginary part appears below k_F owing to the depletion in the occupation of single-particle momentum states. As temperature increases, the size of the imaginary part becomes larger in this region. This is needed since, at very high T, the G matrix should approach the free T-matrix elements, which have a narrow structure in the low-momentum region owing to the existence of a nearly bound state in the $^1S_0$ partial wave. The G matrix for the $^3S_1$ partial wave is shown in Fig. 4. The larger

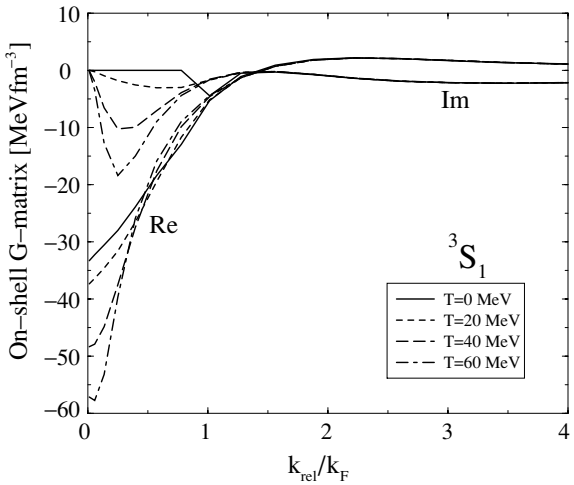

FIG. 4. The same as Fig. 3 for the $^3S_1$ partial wave.

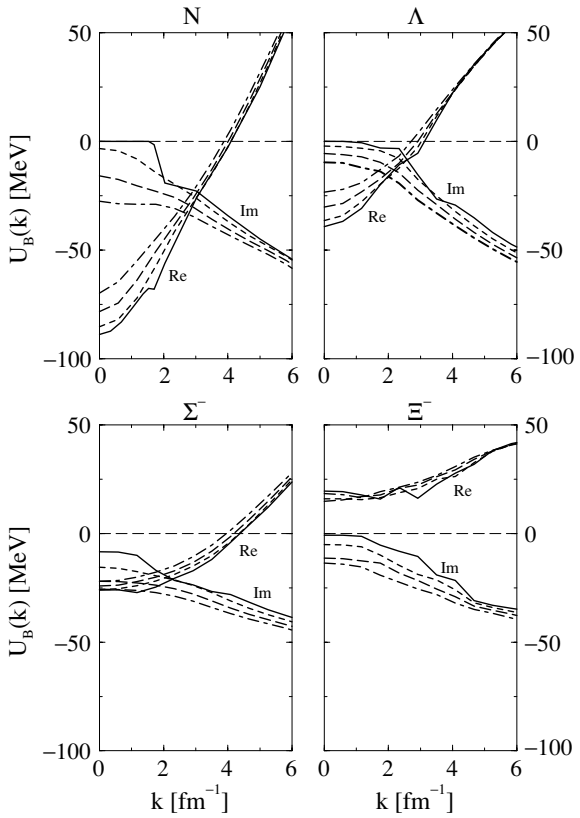

FIG. 5. Single-particle potential of the octet baryons in symmetric nuclear matter at ρ_0 as a function of momentum for various temperatures: $T = 0$ MeV (solid lines), 20 MeV (short-dashed lines), 40 MeV (long-dashed lines), and 60 MeV (dot-dashed lines).

dependence on temperature observed for this partial wave is a direct consequence of the existence of the deuteron pole in the $^3S_1$ T matrix.

Another important quantity, which is directly related to the propagation properties of a baryon B_1 inside a medium of other baryons, is the single-particle potential $U_{B_1}(k)$. In Fig. 5 we display the full momentum dependence of these single-particle potentials for all the octet baryons (N, Λ, Σ, and Ξ) in pure symmetric nuclear matter at normal density ρ_0 for various temperatures. We will first discuss the momentum dependence of the $T = 0$ results. The single-particle potentials at $T = 0$ correspond to the curves that have a stronger structure, owing to more abrupt Pauli blocking and threshold effects. For nucleons, the real part of the single-particle potential shows a cusp around the Fermi momentum, which is a reflection of the in-medium deuteron structure of the $^3S_1$ G-matrix elements. For the Λ and Σ (Ξ) hyperons, the $T = 0$ potential is the one that gives the more attractive (repulsive) potential at the origin. In the particular case of the Λ hyperons, the real part of U_Λ shows a structure around 3 fm^{-1} related to the opening of the ΣN threshold. This is confirmed by the appearance of an additional source of imaginary part in U_Λ around this momentum. The imaginary part of the Σ potential, U_Σ, is already finite at zero momentum owing to its decay through the processes $\Sigma N \to \Lambda N$. Finally, the structures found for the Ξ hyperons around 2 and 3 fm^{-1} reflect the cusps observed in

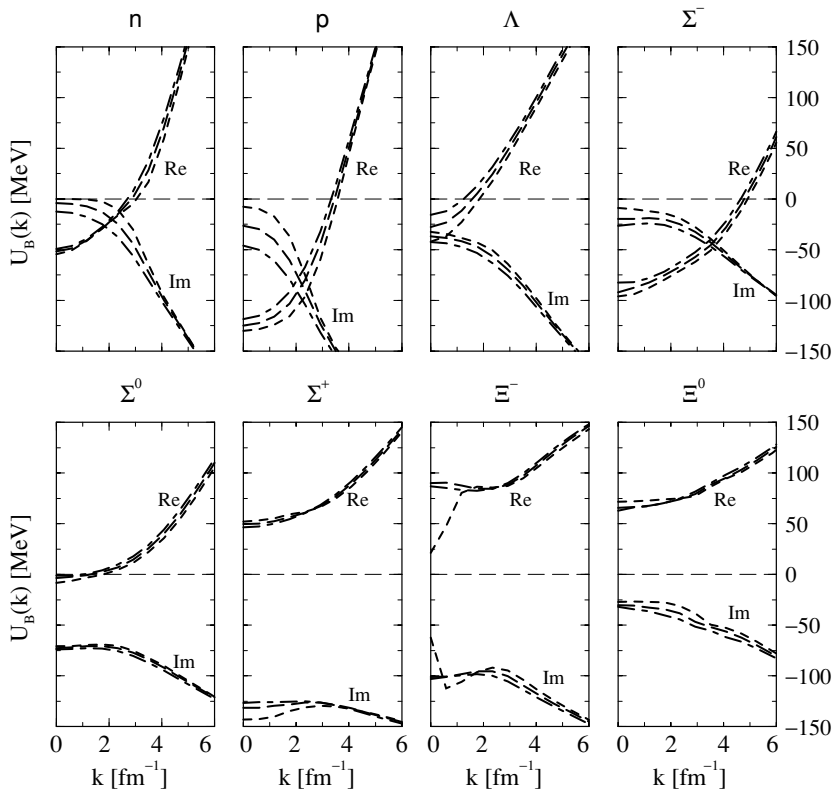

FIG. 6. Single-particle potential of the octet baryons as a function of momentum in baryonic matter at $\rho = 0.5$ fm^{-1} composed by 80% neutrons, 10% protons, and 10% Σ^- hyperons, for various temperatures: 20 MeV (short-dashed lines), 40 MeV (long-dashed lines), and 60 MeV (dot-dashed lines).

the ΞN cross sections at energies corresponding to the opening up of the $\Sigma\Lambda$ and $\Sigma\Sigma$ channels [24], respectively.

With respect to the temperature dependence, we see that the single-particle potentials change gradually as temperature increases. For the momenta explored, the imaginary part of the single-particle potential for all baryons increases in size with temperature, as a consequence of the increase of phase space in the low-momentum region. Temperature effects on the imaginary parts are more important near the origin. When going from $T = 0$ to $T = 60$ MeV, their increase is of the order of 25 MeV for nucleons, 10 MeV for Λs, and 15 MeV for the Σ and the Ξ hyperons. In the nucleon sector, the attractive real part of the single-particle potential becomes less and less attractive as temperature increases (an effect that, near the origin, involves a 20% correction at $T = 60$ MeV with respect to the $T = 0$ MeV result). This may seem contradictory with the small gain in attraction of the *NN* *G*-matrix elements at $T = 60$ MeV, shown in Figs. 3 and 4. Note, however, that the finite-temperature momentum distribution also allows for the contribution of higher relative momentum states to $U(k)$. Since in this region the effective interaction is less attractive, the net effect on $U(k)$ is a loss in the attraction as temperature increases. This is in accordance with what was observed in the pioneering work of Ref. [17]. The real parts of the Λ and Σ single-particle potentials also show the same trend and, at the origin, they increase 30% and 5%, respectively, when the temperature increases from 0 to 60 MeV. However, in contrast to the other baryons, the real part of the Ξ single-particle potential is repulsive and, at zero momentum, the potential experiences an attractive gain of about 2 MeV as temperature is increased.

Next, in Fig. 6, we show the finite-temperature single-particle potentials of all the baryons of the ground-state octet in a baryonic matter of total density $\rho = 0.5$ fm^{-1}. At this density, one expects matter to contain additional degrees of freedom, such as those of hyperons. We have chosen a composition of neutrons, protons, and Σ^- hyperons in proportions of 80%, 10%, and 10%, respectively. This corresponds to a representative example of the composition of a cold neutron star in β equilibrium [15]. This case is interesting because the finite fraction of hyperons makes the properties of matter depend not only on the *NN* interaction but also on both the *YN* and *YY* in-medium effective interactions.

Regarding the momentum dependence, all the single-particle potentials have a steeper growth with respect to the previous case (note the different vertical scale in Fig. 6 compared to that in Fig. 5), in accordance with the fact that the system is at a higher density. The most salient feature is, however, the different behavior of the single-particle potential for the various members of the same isospin multiplet resulting from the strong isospin asymmetry in the composition of matter. As expected, protons become more attractive than neutrons owing to the excess of *np* interacting pairs in the strongly attractive $^3S_1 - {}^3D_1$ $I = 0$ channel. The differences found for the Σ hyperons are also interesting: the Σ^- single-particle potential receives a large contribution from the interaction of $I = 3/2$ $\Sigma^- n$ pairs, which is strongly attractive for the NSC97e model used in this work. Conversely, the repulsive Σ^+ potential is basically built from the interaction of $\Sigma^+ n$ pairs, which, apart from the attractive $I = 3/2$ component, also receive contributions from the very repulsive $I = 1/2$ component of the ΣN NSC97e interaction. Finally, the Σ^0

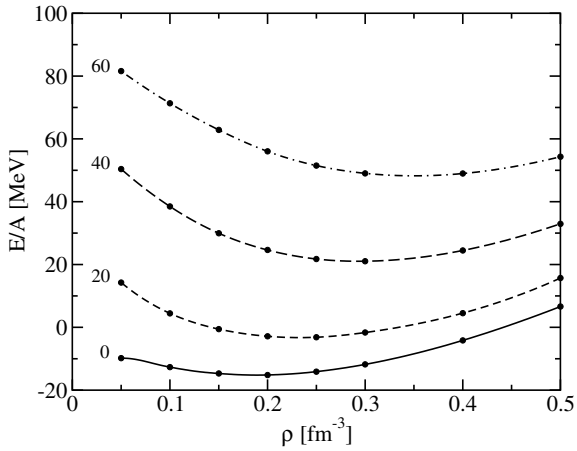

FIG. 7. Energy per nucleon of symmetric nuclear matter as a function of density for various temperatures: 0, 20, 40, and 60 MeV.

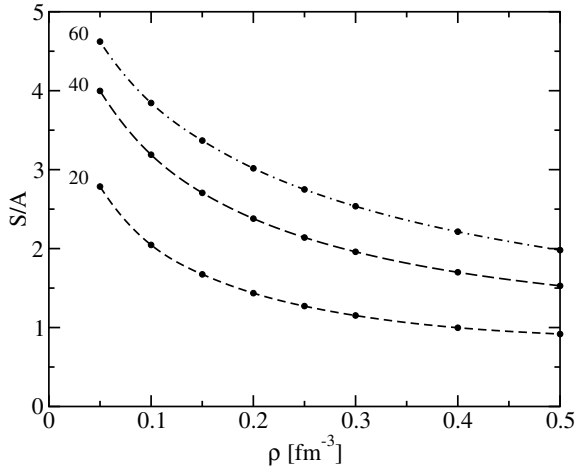

FIG. 8. Entropy per nucleon of symmetric nuclear matter as a function of density for various temperatures: 20, 40, and 60 MeV.

is not affected by the asymmetry between neutrons and protons and its potential is mildly attractive. The single-particle potential of the Ξ^- particle at $T = 20$ MeV shows a strong structure at low momentum, which is also related to the opening of the $\Lambda\Sigma^-$ and $\Sigma^0\Sigma^-$ channels, as discussed in the previous figure for symmetric nuclear matter at $\rho = \rho_0$, but occurring now at lower energy owing to the more attractive single-particle potentials felt by the Λ and the Σ^- at this higher density. This effect is magnified by the relatively larger amount of $\Xi^- n$ interacting pairs in this highly asymmetric baryonic matter containing a neutron fraction of 80%.

With respect to the temperature dependence, for all the baryon species studied, it is found that the attractive single-particle potentials become slightly less attractive and the repulsive potentials become also less repulsive with increasing temperature. In other words, the real parts of the single-particle potential lose strength as temperature increases. It is also interesting to note that, in this case, the single-particle potential of the neutron (which is the most abundant species) is only slightly modified with temperature despite the higher density. In contrast, protons, which are much less abundant, are more affected by temperature, especially the imaginary part of the single-particle potential, which increases by almost 40 MeV when the temperature changes from 20 to 60 MeV. The real part of the Λ single-particle potential at the origin also increases considerably, by almost 30 MeV. For the other particles, except as already noted for the Ξ^-, the changes in the single-particle potential (both real and imaginary parts) amount to 10–15 MeV.

B. Bulk properties

From the astrophysical point of view, the main interest lies in the thermodynamical properties of the extended system of baryons at finite temperature. These are the properties that we will discuss from now on. In Fig. 7, for instance, we report our results for the internal energy per nucleon, E/A, of symmetric nuclear matter as a function of density for various temperatures. At $T = 0$ we can reproduce the saturation properties by implementing an additional TBF on top of the Av18 interaction. We note that E/A increases considerably with temperature for all densities, basically as a result of the increase of kinetic energy. The interacting part of the energy becomes slightly less attractive as temperature rises. For instance, at $T = 60$ MeV the interaction energy is only about 15 MeV higher than in the $T = 0$ case in the whole range of densities explored, whereas the noninteracting part of the internal energy increases an amount that varies between 50 and 90 MeV in the same density range. We also note that the internal energy at $T = 60$ MeV and $\rho = 0.05$ fm^{-3} has practically reached the nondegenerate classical limit ($\varepsilon_F/T = 0.14 \ll 1$), where E/A would amount to $\frac{3}{2}T = 90$ MeV; this occurs because in this case the potential energy is negligible with respect to the kinetic contribution.

The entropy per particle, as calculated from the mean-field-approximation expression of Eq. (9), is displayed in Fig. 8. The values obtained at $T = 20$ MeV are similar to those in the work of Baldo and Ferreira [18], where results for temperatures up to $T = 28$ MeV are reported. As expected, the entropy increases with T. We also observe that, at a given temperature, the entropy is always largest at the lowest density, where one is closer to the classical limit and decreases smoothly with increasing density as the system evolves to the degenerate regime.

In Fig. 9 we show our results for the free energy per nucleon obtained from Eq. (8). For temperatures greater than 20 MeV, and throughout the range of densities explored, the entropic negative contribution, $-TS$, dominates over the internal energy one, E. This is evidently more pronounced at low densities, when one is closer to the classical limit, where the entropy becomes very large. The limited number of temperature values reported in Fig. 9 prevents us from studying the liquid-gas coexistence region. We have performed calculations on a finer grid of temperatures, which clearly reveal that the flashing temperature $T_{\rm fl}$ (i.e., the temperature above which F/A no longer shows a minimum) is around 12 MeV. The critical temperature T_C cannot be obtained from a direct ocular inspection of F/A versus density. However, by

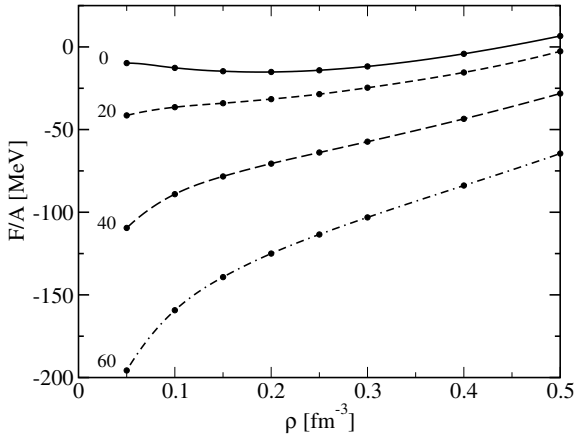

FIG. 9. Free energy per nucleon of symmetric nuclear matter as a function of density for various temperatures: 0, 20, 40, and 60 MeV.

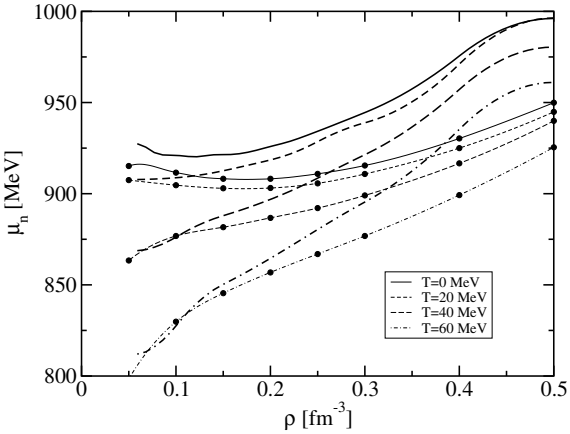

FIG. 10. Nucleon chemical potential for various temperatures as a function of density. The solid circles correspond to the chemical potential $\tilde{\mu}$, obtained from the normalization condition of Eq. (6); the thick lines correspond to μ, the chemical potential obtained from the derivative of the free energy.

calculating numerical derivatives of the free energy we can establish, within the accuracy of our model, that T_C lies in the range 15–20 MeV, a result similar to those obtained in other BHF approaches using different *NN* interactions [18–22].

We recall that in the present study we are using the NTBBG approach, which corresponds to truncating the two-body correlation contribution of the BD diagrammatic expansion of the grand-canonical potential to first order in the two-body scattering matrix. This procedure, valid for low temperatures, is formally analogous to the BHF binding potential of the zero-temperature case in which the Fermi step functions are replaced by the finite-temperature Fermi-Dirac distributions. An explicit calculation allowed the authors of Ref. [18] to conclude that, in the temperature and density range explored in that work, the higher order terms neglected in the finite-temperature expansion represented at most a few percent of the leading term, so they could be safely neglected. Since we are considering here values of temperature of up to about twice the highest temperature explored in Ref. [18], we expect slightly larger errors but not more than 10% of the interaction terms; that is, the higher order contributions would increase the free energy per particle by less than 5 MeV at $T = 60$ MeV.

The chemical potential of the nucleons as a function of density is shown in Fig. 10 for various temperatures. The thick lines correspond to the chemical potential obtained from the derivative of the free energy, Eq. (10); the thin lines, which interpolate the calculated points, represent the chemical potential extracted from the density according to the normalization condition shown in Eq. (6). It is well known that the discrepancies observed from both procedures reflect a violation of the Hugenholtz-Van Hove theorem [31] characteristic of a nonconserving approximation. Those discrepancies arise because, in the BHF method adopted here, the so-called rearrangement terms are absent. Therefore, the single-particle spectrum is, in general, less repulsive and, as a consequence, the chemical potential from the normalization condition is smaller than that obtained using the derivative of the free energy. From Fig. 10 we can see that rearrangement effects are more important at higher densities, being of the order of 50 MeV at the highest density in the $T = 0$ case. Their sizes reduce with increasing temperature and at $T = 60$ MeV they amount to at most 35 MeV. Such a decrease is related to the reduction of medium effects with increasing temperature and, as a consequence, the density dependence of the effective interaction, from which the rearrangement terms originate, becomes also less important.

One may restore the fulfillment of the Hugenholtz-Van Hove theorem by adding the difference of chemical potentials to the BHF single-particle potential energy $U(k)$. This shift will affect the G matrix and, therefore, the Brueckner energy of Eq. (5). However, one should also consistently add the contribution of the bubble and the potential insertion diagrams, which no longer cancel. As pointed out in Ref. [18] this correction compensates quite accurately for the modification of the Brueckner energy at $T = 0$ and, to the extent that the NTBBG is a reasonable approximation at low temperatures, it does not affect our finite-temperature results either. Therefore, our thermodynamical quantities, together with a chemical potential extracted from the derivative of the free energy, can be considered as those of a conserving approximation.

Finally, we present in Figs. 11 to 13 our results for the thermodynamic quantities in the case of baryonic matter with a neutron fraction $x_n = 0.8$, a proton fraction $x_p = 0.1$, and a Σ^- hyperon fraction $x_\Sigma = 0.1$. Although strictly speaking this composition is representative of β-stable hyperonic matter at $T = 0$ and $\rho = 0.5$ fm^{-3}, we have kept it in a wide range of densities and temperatures to see the relevance of having a finite fraction of hyperons on the bulk properties of this hypothetical hadronic matter. The thin lines display the nucleonic-only contribution normalized per baryon, so that we can clearly distinguish the hyperon effects on the thermodynamical properties.

Our results for the internal energy are shown in Fig. 11. We first discuss the behavior of the nucleonic contributions. With this composition, the nucleonic contribution corresponds essentially to that of neutron matter, modified by a 10% proton fraction, which induces the presence of neutron-proton pairs

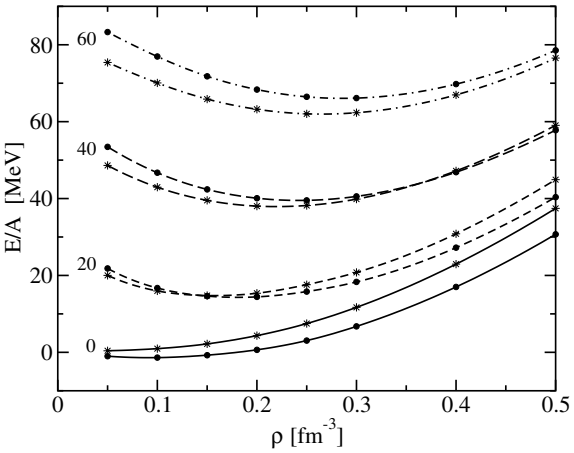

FIG. 11. Internal energy per baryon as a function of density of baryonic matter composed of 80% neutrons, 10% protons, and 10% Σ^- hyperons, for various temperatures: 0, 20, 40, and 60 MeV. The total and nucleonic-only contributions to the internal energy per baryon are denoted by solid circles and stars, respectively.

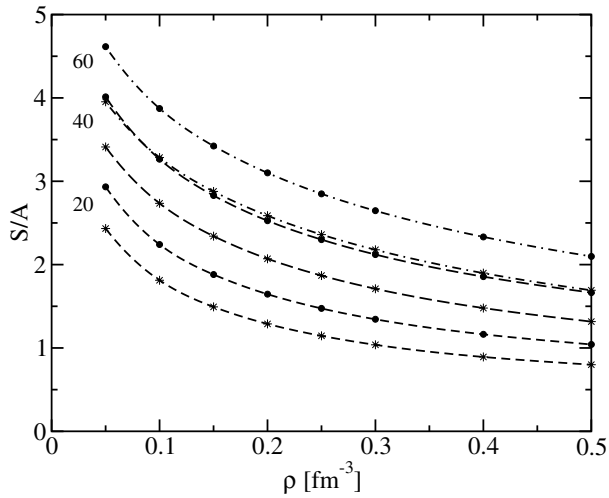

FIG. 12. Entropy per nucleon as a function of density of baryonic matter composed by 80% neutrons, 10% protons, and 10% Σ^- hyperons, for various temperatures: 20, 40, and 60 MeV. The total and nucleonic-only contributions to the entropy per baryon are denoted by solid circles and stars, respectively.

interacting through the very attractive isospin-zero *NN* force. The smooth increase of E with density at $T = 0$ MeV is a result of the combination of the increasing free Fermi gas power law of $\rho^{2/3}$ for $E_{\rm kin}$ with a smooth attractive behavior for $E_{\rm pot}$, which has a saturating minimum of -25 MeV at $\rho = 0.27$ fm^{-3}. As temperature increases, $E_{\rm kin}/A$ increases very rapidly, especially at low densities, where it approaches the classical limit of $\frac{3}{2}Tx_N$. The resulting E/A is then dominated by the noninteracting contribution with some slight modulation from the interaction terms, which increase by about 10 MeV when going from $T = 0$ MeV to $T = 60$ MeV, still maintaining the saturating shape. We now discuss the differences between the thick and thin lines, which are due to the Σ^- hyperonic contributions. At zero temperature, the repulsive hyperonic free Fermi gas contribution is very small compared to the interaction contributions, which come essentially from $\Sigma^- n$ pairs and, to a minor extent, from $\Sigma^-\Sigma^-$ pairs. Both of them interact attractively for the Nijmegen potential used here [24]. Comparing the total internal energy at zero temperature with the nucleonic contribution, one also observes that, as expected for the interaction terms to the energy per baryon of a very diluted system, the size of the attractive hyperonic contribution increases practically linearly with density up to a value of -6 MeV at $\rho = 0.5$ fm^{-3}. At finite temperatures and because of the very low hyperonic density, the kinetic hyperonic component, $E_{\rm kin}/A$, rapidly acquires the classical value of $\frac{3}{2}Tx_Y$ for all densities, whereas the interaction terms depend little on temperature. As a consequence, the hyperonic kinetic energy overcomes the potential energy and the total hyperonic contribution to E/A switches from being attractive to being repulsive when the temperature increases from 0 to 60 MeV. Note, however, that the hyperonic interacting terms still play a role at $T = 60$ MeV and should not be neglected. At twice normal nuclear matter density and $T = 60$ MeV, they represent about half of the hyperonic kinetic energy contribution.

The entropy per baryon is represented in Fig. 12. As expected, the total entropy per baryon decreases smoothly with increasing density as one moves away from the classical limit. By comparing the total (thick lines) with the nucleonic-only (thin lines) contributions we observe a strong influence of the hyperons in the final value of the entropy, despite their mere 10% fraction of the total number of particles. This effect on entropy occurs because the hyperons in this system form a very diluted gas, which behaves almost classically and hence has large entropy values.

From the internal energy and the entropy shown in the Figs. 11 and 12, one derives the free energy displayed in Fig. 13. We observe that the hyperonic contributions decrease the free energy at all temperatures and densities. This effect

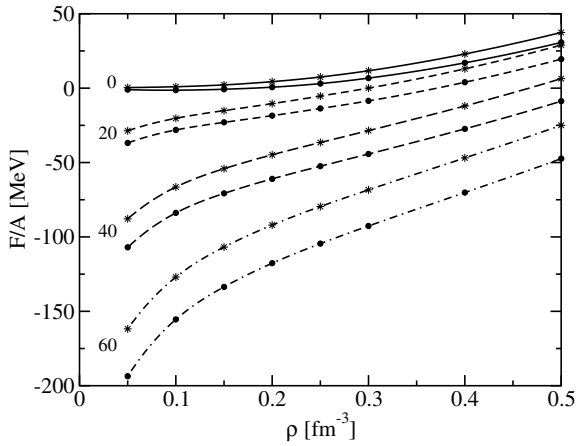

FIG. 13. Free energy per nucleon as a function of density of baryonic matter composed by 80% neutrons, 10% protons, and 10% Σ^- hyperons, for various temperatures: 0, 20, 40, and 60 MeV. The total and nucleonic-only contributions to the free energy per baryon are denoted by solid circles and stars, respectively.

is more pronounced at higher temperatures, for which the negative entropic term of the free energy dominates. However, for a given temperature the shift in the free energy per particle is almost independent of the density.

IV. CONCLUSIONS

In the present work we have studied hadronic matter at finite temperature and density within the NTBBG approach using the Argonne V18 potential plus a three-body force for the nucleon-nucleon interaction and the Nijmegen NSC97e potential for the hyperon-nucleon (*YN*) and hyperon-hyperon (*YY*) ones. To our knowledge, this is the first time that a fully microscopic calculation of matter with hyperons has been performed at finite temperature.

In this approximation, the single-particle occupation probabilities are replaced by thermal Fermi distributions. This affects the Pauli blocking factor on the intermediate states appearing in the equation that defines the in-medium effective interaction. With increasing temperature, the Pauli blocking loses strength and the interaction, which shows in general a moderate temperature dependence, tends to acquire the behavior observed for the corresponding free T matrix.

We have obtained the single-particle potentials of all the baryons for various temperatures in two different cases: symmetric nuclear matter at normal density and a system composed by 80% neutrons, 10% protons, and 10% Σ^- hyperons at a density of $\rho = 0.5$ fm^{-3}, which is representative of a β stable composition of a neutron star. Temperature effects on the single-particle potentials are at most of the order of 25% when the temperature increases from 0 to 60 MeV in all the baryons, being more relevant for the imaginary parts, which increase in size owing to the gain in phase space. With increasing temperature, the size of the real part of the potential at zero momentum decreases (independently of whether it is attractive or repulsive) as a results of the contribution of higher momentum components for which the effective interaction is weaker.

We have also studied the dependence with density and temperature of the bulk properties of hadronic matter, namely, the energy, entropy, and free energy.

In the case of symmetric nuclear matter we have checked that our results are very similar to the previous available calculations [18]. Although the kinetic terms play an increasing role with increasing temperatures, the final value of the thermodynamical quantities is, in the range of densities and temperatures explored in this work, substantially affected by the interacting terms. We have compared the values of the chemical potential obtained from the density normalization and from the derivative of the free energy to have an estimate of the rearrangement terms neglected in the NTBBG approach. It is found that the rearrangement effects increase with density and decrease with temperature. We note, however, that the bulk thermodynamical quantities are little affected by these missing rearrangement components in the single-particle spectrum [18].

We have also analyzed the relevance of hyperonic contributions to the bulk properties of matter by fixing the composition to 80% neutrons, 10% protons, and 10% Σ^- and varying the density and temperature. Because of the small fraction of hyperons considered, the Σ^- start behaving classically for low densities. Thus the kinetic contribution to the energy easily overcomes the *YN* and *YY* potential energy contributions. However, the latter cannot be neglected since it represents about half of the hyperonic kinetic contribution at the largest temperature of $T = 60$ MeV explored in this work. In addition, we see that the entropy of the hadronic system is very sensitive to the presence of the Σs, despite their relatively low fraction. Although the deviations with respect to the nucleonic sector are more important for higher temperatures, they do not depend on density. We also find that the modest presence of hyperons leads to substantial reduction of the free energy, obviously associated with the increase of entropy.

As we have already pointed out, to our knowledge, this is the first microscopic calculation of the finite-temperature EoS of dense baryonic matter including degrees of freedom other than nucleons. It represents a first step in the microscopic study of hadronic matter at finite temperature, which is of great importance, on one hand, for a proper understanding of supernova and proto-neutron star physics and, on the other, for the analysis of heavy-ion collision data.

ACKNOWLEDGMENTS

We acknowledge fruitful discussions with Marcello Baldo. This work is partly supported by DGICYT Contract No. BFM2002-01868 and the Generalitat de Catalunya Contract No. SGR2001-64. This research is part of the EU Integrated Infrastructure Initiative Hadron Physics Project under Contract No. RII3-CT-2004-506078. Arnau Rios acknowledges the support from DURSI and the European Social Funds.

[1] D. H. Rischke, Prog. Part. Nucl. Phys. **52**, 197 (2004).
[2] U. W. Heinz, J. Phys. G **31**, S717 (2005).
[3] D. d'Enterria, Invited talk to appear in the Proceedings of the 39th Rencontres de Moriond on QCD and High-Energy Hadronic Interactions, La Thuile, Vallee d'Aoste, 28 March–4 April 2004; nucl-ex/0406012.
[4] M. Prakash, I. Bombaci, M. Prakash, P. J. Ellis, J. M. Lattimer, and R. Knorren, Phys. Rep. **280**, 1 (1997); H. Heiselberg and M. Hjorth-Jensen, *ibid.* **328**, 237 (2000).
[5] S. Balberg and A. Gal, Nucl. Phys. **A625**, 435 (1997).
[6] S. Balberg, I. Lichtenstadt, and G. B. Cook, Astrophys. J. Suppl. **121**, 515 (1999).
[7] N. K. Glendenning, Astrophys. J. **293**, 470 (1985).
[8] R. Knorren, M. Prakash, and P. J. Ellis, Phys. Rev. C **52**, 3470 (1995).
[9] J. Schaffner and I. N. Mishustin, Phys. Rev. C **53**, 1416 (1996).

[10] L. Yang, W. L. Qian, R. K. Su, and H. Q. Song, Phys. Rev. C **70**, 045207 (2004).
[11] H.-J. Schulze, A. Lejeune, J. Cugnon, M. Baldo, and U. Lombardo, Phys. Lett. **B355**, 21 (1995).
[12] H.-J. Schulze, M. Baldo, U. Lombardo, J. Cugnon, and A. Lejeune, Phys. Rev. C **57**, 704 (1998).
[13] I. Vidaña, A. Polls, A. Ramos, M. Hjorth-Jensen, and V. G. J. Stoks, Phys. Rev. C **61**, 025802 (2000).
[14] M. Baldo, G. F. Burgio, and H.-J. Schulze, Phys. Rev. C **61**, 055801 (2000).
[15] I. Vidaña, A. Polls, A. Ramos, L. Engvik, and M. Hjorth-Jensen, Phys. Rev. C **62**, 035801 (2000).
[16] I. Vidaña, I. Bombaci, A. Polls, and A. Ramos, Astron. Astrophys. **399**, 687 (2003).
[17] A. Lejeune, P. Grangé, M. Martzolff, and J. Cugnon, Nucl. Phys. **A453**, 189 (1986).
[18] M. Baldo and L. S. Ferreira, Phys. Rev. C **59**, 682 (1999).
[19] M. Baldo, I. Bombaci, L. S. Ferreira, G. Giansiracusa, and U. Lombardo, Phys. Lett. **B215**, 19 (1988).
[20] I. Bombaci, T. T. S. Kuo, and U. Lombardo, Phys. Lett. **B311**, 9 (1993).
[21] W. Zuo, Z. H. Li, A. Li, and G. C. Lu, Phys. Rev. C **69**, 064001 (2003).
[22] M. Baldo, L. S. Ferreira, and O. E. Nicotra, Phys. Rev. C **69**, 034321 (2004).
[23] R. B. Wiringa, V. G. J. Stoks, and R. Schiavilla, Phys. Rev. C **51**, 38 (1995).
[24] V. G. J. Stoks and Th. A. Rijken, Phys. Rev. C **59**, 3009 (1999).
[25] H. Q. Song, M. Baldo, G. Giansiracusa, and U. Lombardo, Phys. Rev. Lett. **81**, 1584 (1998).
[26] M. Baldo, G. Giansiracusa, U. Lombardo, and H. Q. Song, Phys. Lett. **B473**, 1 (2000).
[27] Th. A. Rijken, V. G. J. Stoks, and Y. Yamamoto, Phys. Rev. C **59**, 21 (1998).
[28] A. L. Fetter and J. D. Walecka, *Quantum Theory of Many Particle Physics* (McGraw-Hill, New York, 1971).
[29] For a recent review see P. A. Hening, Phys. Rep. **253**, 235 (1995).
[30] C. Bloch, Nucl. Phys. **7**, 451 (1958); C. Bloch and C. De Domicis, *ibid*. **7**, 459 (1958); **10**, 181 (1959); **10**, 509 (1959).
[31] N. M. Hugenholtz and L. Van Hove, Physica (Utrecht) **24**, 363 (1958).